IEEE Access
Multidisciplinary | Rapid Review | Open Access Journal

Received January 20, 2021, accepted February 2, 2021, date of publication February 8, 2021, date of current version February 16, 2021.

*Digital Object Identifier 10.1109/ACCESS.2021.3057848*

# A Broadband Ultra-Thin Polarization Rotator Using Periodically Loaded Parallel Strip-Lines

**XIAOMING LIU[1,2], (Member, IEEE), TAO QI[1], CHEN WANG[1], XIAOFAN YANG[3], LU GAN[1,2], AND QING CAI[4]**

[1]School of Physics and Electronic Information, Anhui Normal University, Wuhu 241002, China
[2]Anhui Provincial Engineering Laboratory on Information Fusion and Control of Intelligent Robot, Wuhu 241002, China
[3]State Key Laboratory of Complex Electromagnetic Environment Effects on Electronic and Information System, Luoyang 471004, China
[4]Shanghai Institute of Measurement and Testing Technology, Shanghai 201203, China

Corresponding author: Xiaoming Liu (xiaoming.liu@ahnu.edu.cn)

This work was supported in part by the National Natural Science Foundation of China under Grant 61871003, and in part by the open project of the state key laboratory of complex electromagnetic environment effects on electronics and information system under Grant CEMEE2021Z0201B.

**ABSTRACT** A polarization rotator based on loaded parallel strip-lines is theoretically and experimentally investigated. The unit cells are short-stub loaded parallel strip-lines. The arrays on the front and back layers are rotated by 90° to each other. By loading the stubs, good coupling between the two layers is obtained. Such a structural rotation along with the loading stubs allow the *y*-polarized wave to be converted to *x*-polarized wave through field coupling. A broad transmission bandwidth of 30% (86-116 GHz) by using the proposed structure has been reached. In addition, the PTFE substrate is only 0.25 mm thick, which is less than 0.1λ at 86 GHz. Such a thickness allows the polarization rotator to be easily mounted on antenna radomes. The fabricated prototype demonstrates good agreement between simulation and measurement results.

**INDEX TERMS** Polarization rotator, periodical structure, strip-lines, wideband, angular stability.

## I. INTRODUCTION

Periodical structures have been intensively investigated for a broad range of applications, such as frequency selective surface (FSS) [1], radar antenna radomes [2], antenna gain enhancement [3], [4], absorber [5], [6] and so forth. They are also used to manipulate polarization [7]–[16], generating orbital angular momentum [17], [18], and are consequently employed in many remote sensing [19] and communication [20] systems.

A polarization rotator rotates the linearly polarized incident wave by a certain angle, in most cases 90°. There are largely two catalogues of polarization rotator, i.e., the reflection type [7]–[13] and the transmission type. For the reflection type, oblique incidence is required in order to avoid blockage by the radiating source. The transmission type [21]–[24] is widely used in applications where polarization separation is demanded. To fulfill this functionality, there are a good versatile of designs, such as the substrate integrated waveguide (SIW) [21], slant lines [22], coupling slots array [23], and so on. The SIW structure requires many shorting pins, which inevitably increases the fabrication cost and is less suitable for millimeter wave range, though good performance may be obtained. Slant line structure requires multi-layer structure to achieve satisfactory bandwidth. Coupling slots array does not show very good bandwidth or angular stability.

This paper reports a transmission type ultra-thin polarization rotator using periodically loaded parallel strip-lines, for the application of a 94 GHz imaging system requiring a minimal bandwidth of ±5 GHz. Only one substrate is used in this design, and both sides are patterned with unit cells. The unit cells on the back layer are rotated by 90° with regard to the front layer to obtain polarization rotation. By introducing a stub on the strip, good coupling can be achieved. Compared to other types of polarization rotator, low profile, easy fabrication and good bandwidth are observed. Particularly, the PTFE substrate is only 0.25 mm thick, making it easy to be mounted on many antenna systems. In addition, only one substrate is needed and common PCB etching technique is competent to fabricate such structure. Furthermore, this structure produces satisfactory angular stability.

The following parts are organized as follows: Section II is devoted to the theory and design, Section III presents the

The associate editor coordinating the review of this manuscript and approving it for publication was Jaime Laviada.

This work is licensed under a Creative Commons Attribution-NonCommercial-NoDerivatives 4.0 License.
For more information, see https://creativecommons.org/licenses/by-nc-nd/4.0/

fabrication and measurement, and Section IV summarizes this work.

## II. THEORY AND DESIGN

### A. DESIGN CONSIDERATIONS

Suppose a train of vertically polarized EM wave, when incident on a rotator, its polarization should be rotated by a certain angle $\theta$. As an example, the EM wave is rotated from vertical polarization to horizontal polarization, as shown in Fig. 1. The front layer can be considered as a receiving array, and the back layer is equivalent to a radiation array. Through coupling between the front and back layers, the power can be transmitted from the front side to the back side. To achieve polarization rotation, the current distribution on the back layer should be rotated with respect to the front layer by the same angle. Therefore, the structure on the back layer should be identical to that on the front layer, but rotated by an angle of 90°.

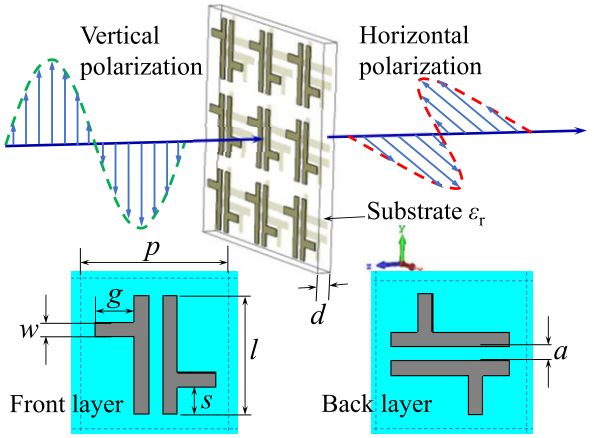


**FIGURE 1. An illustration of polarization rotation from vertically polarized state to horizontally polarized state.**

Using the mathematical description, the output field can be calculated by the transmission matrix

$$\begin{bmatrix} E_{ox} \\ E_{oy} \end{bmatrix} = \begin{bmatrix} T_{xx} & T_{xy} \\ T_{yx} & T_{yy} \end{bmatrix} \begin{bmatrix} E_{ix} \\ E_{iy} \end{bmatrix}. \quad (1)$$

If the incident field is polarized along the $y$ axis, then one has

$$\begin{cases} E_{ox} = T_{xy} E_{iy} \\ E_{oy} = T_{yy} E_{iy}. \end{cases} \quad (2)$$

Therefore, the transmission coefficient $T_{xy}$ is preferred to be close to unity (0 dB) and $T_{yy}$ close to 0 though not possible.

In the design of an FSS, slot array is a type of bandpass filter, and the patch (strip) array functions as a band rejection filter. In this regard, the slot array is usually used in design of bandpass polarization rotator [23], [24]. Actually, the polarization rotation takes place when the current induced by the incident wave can be rotated by 90° on the exit array. Therefore, two conditions may be considered to guide the design. One is the structural rotation between the incident layer and the exit layer, the other is a sufficient strong coupling between these two layers.

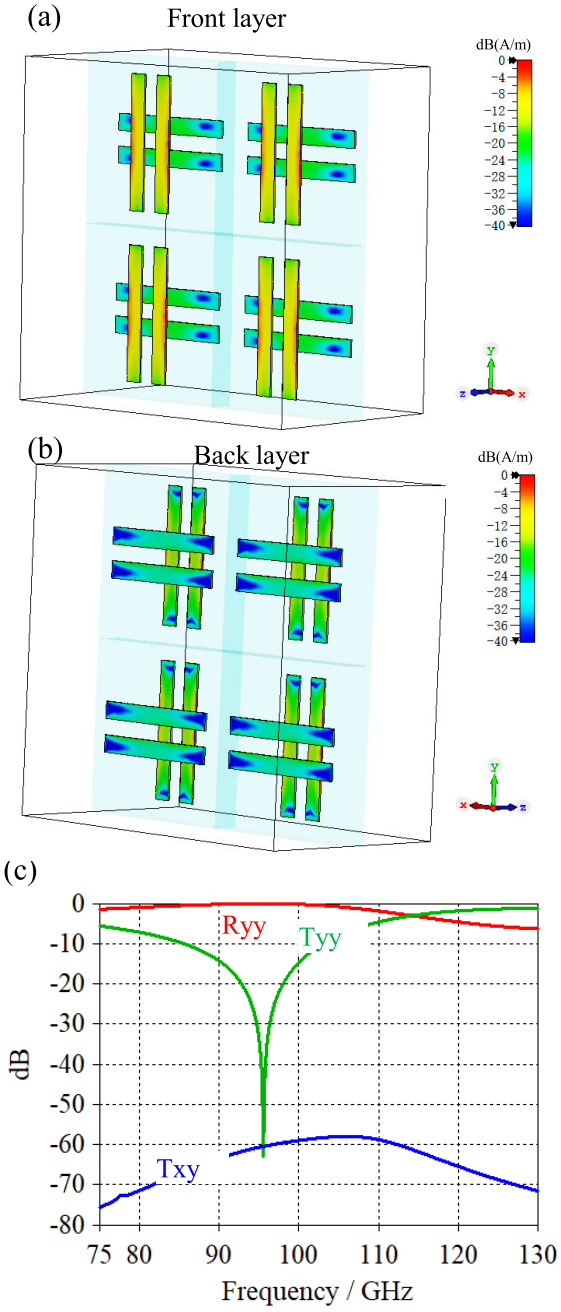


**FIGURE 2. Response of two-trip array. (a) Current on the front layer; (b) current on the back layer; (c) $T_{xy}$, $T_{yy}$ and $R_{yy}$ of this structure.**

The simplest structure is a vertical metal strip on the front layer and a horizontal strip on the back layer. Such a structure, however, does not produce very good coupling, as shown in Fig. 2. The conversion from y-polarization to $x$-polarization is almost null. Therefore, the transmission coefficient $T_{xy}$ is very small, below -50 dB as shown in Fig. 2. Even using the slot array [24], the rotation of structure by 90° does not guarantee a good polarization rotator. This is due to that the current on the front layer cannot be coupled to the back layer. Therefore, a good coupling route has to be created so as to enable this function.

In order to enhance the coupling, a stub has been added near the end of each strip, considering that the stub can change the direction of current. By loading the stub, the coupling effect is greatly enhanced. The position of the stub is defined by $s$ as shown in Fig.1.

To determine the initial value of each parameter, the following methods may be employed. The length of each strip shall be approximately half a wavelength. For a substrate supported strip line, $l \approx \lambda_g/2$, and $\lambda_g$ is the equivalent wavelength

$$\lambda_g = \frac{\lambda_0}{\varepsilon_{\text{eff}}} = \frac{c}{f_0 \varepsilon_{\text{eff}}}, \tag{3}$$

where, $\varepsilon_{\text{eff}}$ is the effective dielectric [25]. The available minimal thickness of the substrate is 0.25 mm. Other parameters are limited by $2(g + w) + a < p$.

Through optimization, the best structure can be achieved. The final structure of the unit cell is shown in Fig. 1, and the optimized parameters are listed in Table 1. The current distribution on each layer is plotted in Fig. 3. It is seen that the major area of current distribution on the front layer is on the vertical strip and the connection part between the vertical strip and the stub, and for the back layer the major area is on the horizontal strip and the connection part between the horizontal strip and the stub. Coupling between the front layer and the back layer takes place at the connection area.

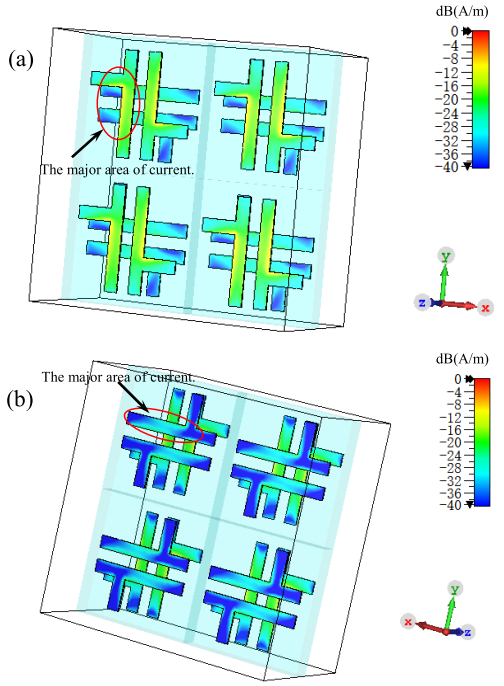


**FIGURE 3.** Current distribution at 94 GHz on (a) the front layer; (b) the back layer.

The simulated results are presented in Fig.4, where the 8 parameters are all plotted. It is seen that for the $x$-polarized wave, the reflection coefficient $R_{xx}$ is very high over the simulated frequency range of 75-130 GHz. It is almost -1 dB in the central range, indicating that the $x$-polarized wave cannot be transmitted through this structure. Therefore, in later discussion, we only use the $y$-polarized wave for incidence. For the $y$-polarized wave, $R_{yy}$ is sufficiently small in the central frequency range, smaller than -10 dB. And the $T_{xy}$ is as good as -1 dB, showing that polarization rotation takes place for the $y$-polarized wave.

**TABLE 1.** Key parameters of the polarization rotator.

| $d$ | $w$ | $l$ | $g$ | $p$ | $s$ | $a$ |
|---|---|---|---|---|---|---|
| 0.25 | 0.15 | 1.2 | 0.39 | 1.5 | 0.27 | 0.14 |

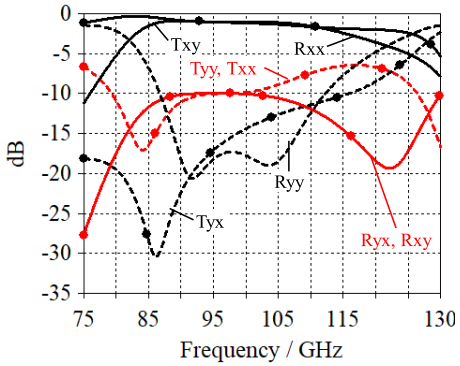


**FIGURE 4.** Simulated results of the optimized structure at normal incidence.

An equivalent circuit model for the polarization is shown in Fig.5. A trip line can be modelled using a series inductor $L$ and capacitor $C_L$ [26]. The end stub can be considered as a capacitor $C_E$ [25]. The coupling can be described using $C_{xy}$, and the dielectric usually shows a transmission line property, denoted by a phase shifter [27]. Since the $y$-polarized wave will be rotated to $x$-polarized wave. The coupling from input port $y$ to output port $y$ should be null. Similarly, coupling from the input port for $x$ to the circuit should be null since the transmission coefficients for $x$ polarized wave is very large.

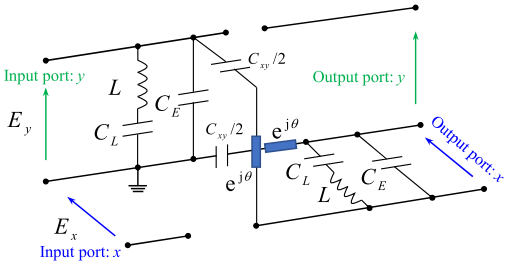


**FIGURE 5.** An ideal equivalent circuit model for the polarization rotator.

### B. PARAMETRIC STUDY

In order to investigate the sensitivity and influence of each parameter, as well as to shed some light on the working principle, a systematic parametric study has been conducted. We set the sweep step to 10 $\mu$m, which is actually the fabrication accuracy. Also, the dielectric permittivity is studied since this parameter is frequency dependent [28] and will also create adverse effect on the performance.

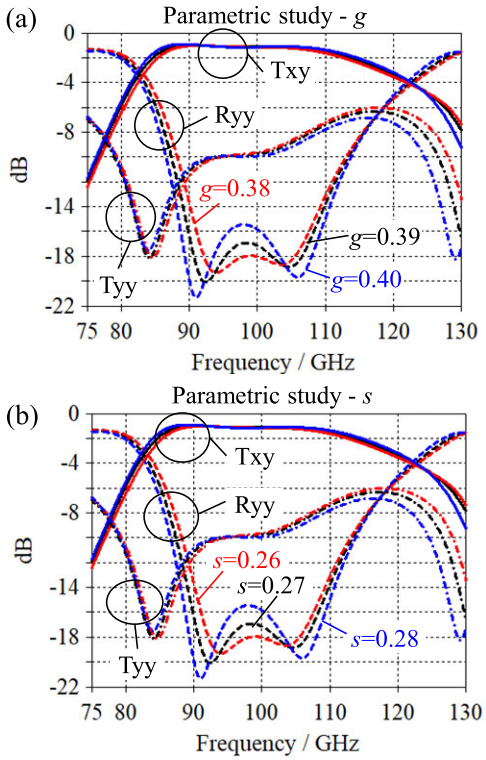


**FIGURE 6.** Parametric study of the stub (a) *g* and (b) *s*.

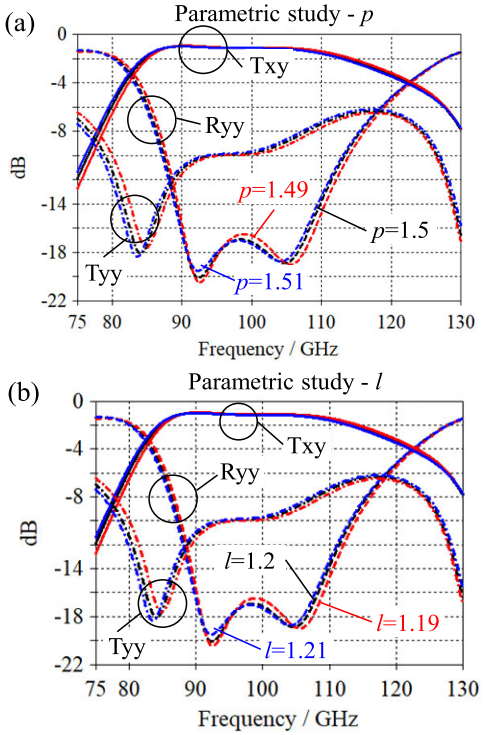


**FIGURE 7.** Parametric study of the unit cell (a) *p* and (b) *l*.

Since the stub plays a critical role in this design, the length of the stub $g$ and the position $s$ are investigated first and the results are shown in Fig.6(a) and Fig.6(b). It is seen that increasing $g$ will broaden the bandwidth and increase the amplitude of the reflection coefficients. The central frequency also undergoes slight shift to lower frequency side. This is due to that the length of the stub will affect the current path. Variation of $s$ within the fabrication accuracy does not affect the response significantly. This may be explained by the current distribution in Fig.3, where the coupling takes place at the connection part, while the end of each strip does not have very strong current distribution.

The length of the unit cell $p$ and the length of the strip $l$ less sensitive to the small variation in length (10 $\mu$m), as shown in Fig. 7.

The parameter $w$ and $d$ do not produce too much effect on the response, as shown in Fig. 8(a) and Fig.8 (b). This is reasonable since the width of each strip does not affect the current path too much. The thickness $d$ does affect the relative permittivity by the microstrip line theory, however not so noticeably in this case. It is seen from Fig.8(c) that higher permittivity will redshift the central frequency. In this design, the provided permittivity is 2.65.

The angular stability is shown in Fig. 9(a). It is seen that the bandwidth is not affected remarkably. The transmission from $y$-polarization to $y$-polarization is slightly increased. Such results indicate very good angular stability, at least up to 30° incident angle. In many systems, this angle is sufficiently large for oblique incidence. For systems of normal incidence, it provides very large margin for components positioning.

It is noted from Fig.9(a) that there is a second resonance near 80.4 GHz. In order to investigated the origin of this resonance, the current distribution at 80.4 GHz is simulated. It is well recognized that there is another current path at the strip line on the opposite part of the stub as indicated in Fig.9(b). The second resonance may be attributed to this additional current path.

## III. FABRICATION AND MEASUREMENTS

The fabricated polarization rotator is shown in Fig.10 (a) and Fig.10(b). The substrate is PTFE of 0.25 mm thick. The fabricated dimensions are 280 mm long and 200 mm wide. The substrate was first cut using a high-precision six-axis drilling/milling machine (HANS-F6M). And then, the pattern was etched out using the etching process. Surface quality control process was employed during fabrication. By using an industry microscope (*SuperEye*), the fabrication accuracy can be examined and measured after calibration. The key parameters are marked using the rule tool of the microscope. It can be seen that the fabrication accuracy is within 5 $\mu$m, better than the expected value of 10 $\mu$m. Such accuracy is sufficiently good, as can be seen from the plots in the parametric study section.

Measurement was conducted using a quasi-optical bench, as shown in Fig.11. The system was connected to a pair of W-band extenders (*VDI WR-10+*). The extenders were driven using a VNA (Cyear AV3276D). A pair of corrugated horns were used for creating Gaussian beam and for receiving

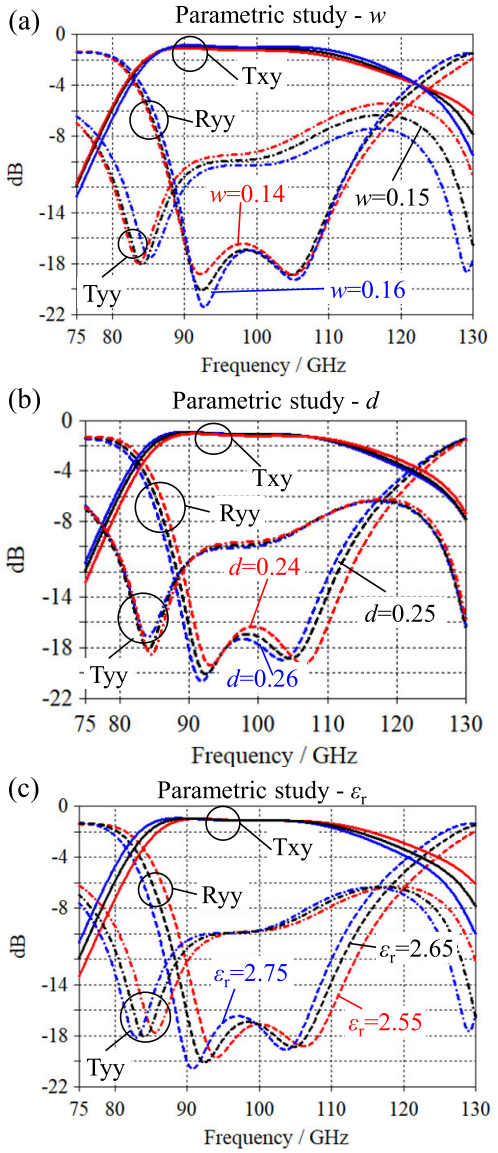


**FIGURE 8.** Parametric study. (a) $w$; (b) $d$; (c) $\varepsilon_r$.

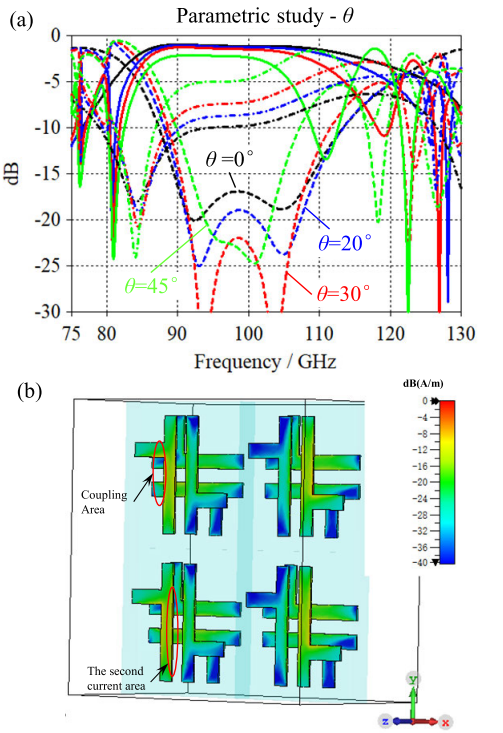


**FIGURE 9.** Angular stability study. (a) Angular dependent response; (b) current distribution at 80.4 GHz with 20° incidence.

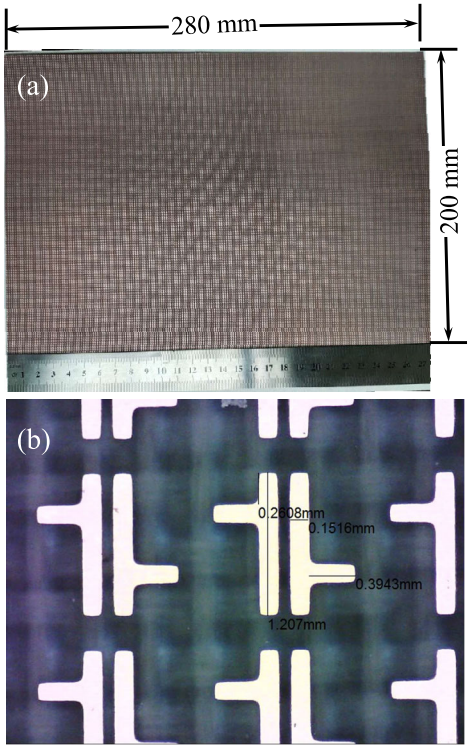


**FIGURE 10.** The fabricated polarization rotator. (a) photograph; (b) photograph under an industrial microscope.

signal. Two ellipsoidal mirrors were employed to refocus the divergence beam, generating a planar wave front at the location of the sample holder. The detailed description of the quasi-optical system is directed to reference [29]. Radar absorption material (RAM) was mounted on the horns to reduce standing waves. Locating holes were drilled to precisely determine the incident angle. A slot calibration was first conducted between the W band extenders. In order to eliminate residual noise, time-gating technique was applied.

The first measurement was conducted on air as background, and the transmission coefficient $S_{21\_air}$ was recorded. After that, the sample was presented for measurement. Three parameters are measured, the transmission from $y$- polarization to $y$- polarization $T_{yy}$, the transmission from $y$-polarization to $x$-polarization $T_{xy}$ and the reflection from $y$-polarization to $y$-polarization $R_{yy}$. For $T_{yy}$, the transmission coefficient for sample $S_{21\_yy}$ was recorded, and therefore $T_{yy} = S_{21\_yy} - S_{21\_air}$. To measure $T_{xy}$, the receiving horn and extender have to be rotated by 90°. The reflection background was measured by placing a metallic plate at the location of

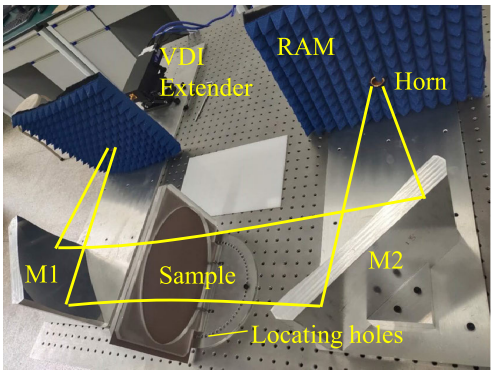


**FIGURE 11.** The Measurement set up using a quasi-optical bentch.

the sample. By fixing the sample holder to different locating holes, the incident angle can be changed.

The measured results are plotted in Fig. 12. It is seen that the measured results are slightly redshifted. But overall, the agreement between simulation and measurement is sufficiently good. Ripples can be observed in the transmission band, with the average insertion loss being 1.5 dB. Ripples are caused by residual scattering of the reflectors and multi reflections of the horns. The reflection s11(y->y) is below -15 dB, and the transmission coefficient s21(y->y) is nearly -10 dB. These results demonstrate that the conversion from the $y$-polarized wave to $x$-polarized wave has been realized through this very simple structure. In addition, the angular stability is also good enough, showing 20° stability. It is also observed that an irregular point exists near 80.4 GHz by simulation. And the measurement of this point takes place near 83-85 GHz. With the increase in the angle of incidence, the irregular point becomes more apparent. Fortunately, this irregular point does not lie in the frequency region of polarization rotation. In this connection, the presence of this point does affect the performance significantly.

The phase of $T_{xy}$ at normal incidence is compared and shown in Fig. 12(d). It is seen that the measurement is in agreement with simulation within 8 degree. The linearity is excellent and good group delay can be derived.

Actually, the bandwidth can also be defined using the polarization conversion ratio (PCR) as defined in [30]. The angular dependent PCR is plotted in Fig.13. It is clear that the bandwidth for 0.707 PCR can be maintained between 88-106GHz. For 0.8 PCR, the bandwidth is 90-105GHz. Tabulated data are listed in Table 2.

**TABLE 2.** Tabulated data for PCR at normal incidence.

| Freq/GHz | 85 | 90 | 95 | 100 | 105 | 110 |
|---|---|---|---|---|---|---|
| Sim. | 0.69 | 0.88 | 0.88 | 0.87 | 0.87 | 0.86 |
| Meas. | 0.63 | 0.87 | 0.89 | 0.88 | 0.85 | 0.85 |

In addition, this structure can also be studied in terms of the Brewster angle by using $\varphi_B = \arctan\left(\sqrt{\varepsilon_s/\varepsilon_{air}}\right)$, as shown in [30]. Since the relative permittivity of the substrate $\varepsilon_s$ is

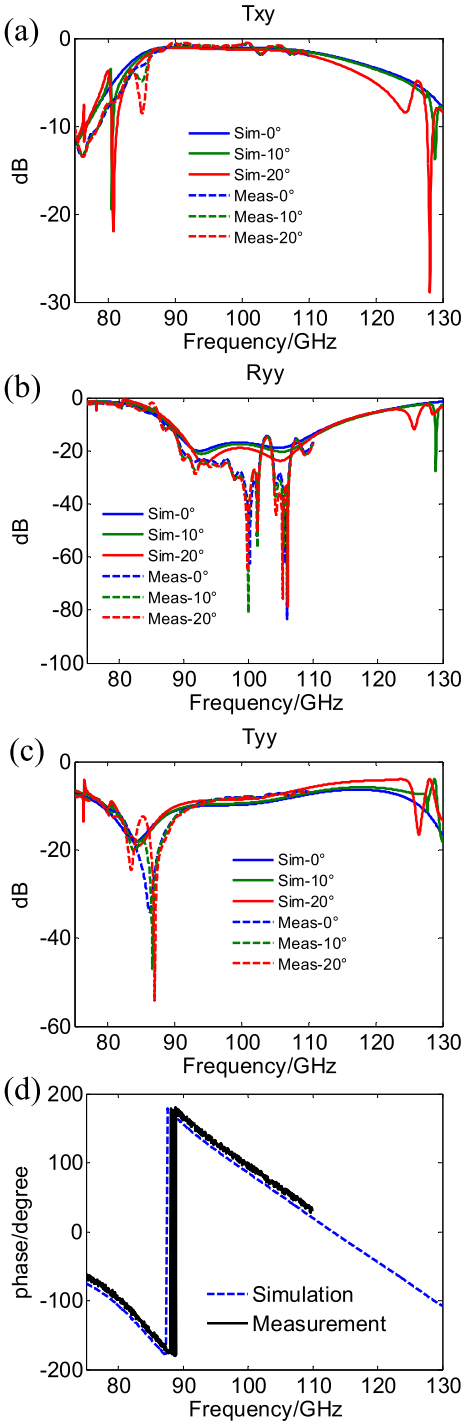


**FIGURE 12.** Measurement results. (a) $T_{xy}$; (b) $T_{yy}$; (c) $R_{yy}$; (d) comparison of the $T_{xy}$ phase at normal incidence.

2.65 and it is 1 for air, the Brewster angle $\varphi_B$ finds to be 58°. It implies that it is possible to separate two orthogonal components when an un-polarized light is incident on the top layer at 58°.

In Table 3, a comparison of the transmission type polarization rotator is presented. It is seen that for single layer structure, this work gives a good tradeoff between number of substrate layer, bandwidth and thickness.

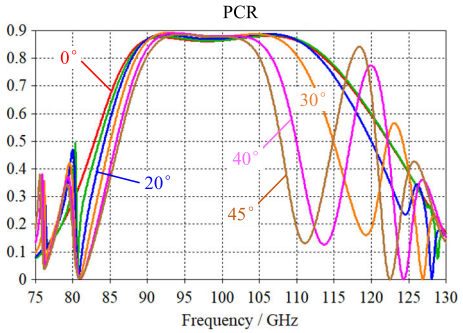


**FIGURE 13.** angular dependent PCR.

**TABLE 3.** Comparison of the performance of existing polarization rotators.

| Ref. | PCR | PCR BW (%) | Layer | Thickness |
|---|---|---|---|---|
| [21] | >0.92 | 10% | 2 | 0.15λ |
| [22] | >0.70 | 15% | 3-4 | 0.13λ |
| [23] | >0.90 | 8% | 1 | 0.053λ |
| [24] | >0.92 | 10% | 2 | 0.95λ |
| [30] | >0.93 | 75% | 3 | 0.15λ |
| [31] | >0.92 | 8% | 2 | 0.2λ |
| This work | >0.85 | 30% | 1 | 0.1λ |

## IV. CONCLUSION

A very simple structure for the applications of millimeter wave polarization rotator has been realized. The unit cell consists of a pair of loaded strip lines. The stub is designed so as to increase the coupling between the incident and exit polarizations. The structure on the front and back layers are rotated by 90° to each other. Substrate thickness is only 0.1λ at 86 GHz, showing a very thin design. The rotator works at 86-116 GHz, indicating a broadband property. Good angular stability can be maintained from 90-105 GHz.

## REFERENCES

[1] W. Yin, H. Zhang, T. Zhong, and X. Min, "Ultra-miniaturized low-profile angularly-stable frequency selective surface design," *IEEE Trans. Electromagn. Compat.*, vol. 61, no. 4, pp. 1234–1238, Aug. 2019, doi: 10.1109/TEMC.2018.2881161.

[2] A. A. Omar and Z. Shen, "Thin 3-D bandpass frequency-selective structure based on folded substrate for conformal radome applications," *IEEE Trans. Antennas Propag.*, vol. 67, no. 1, pp. 282–290, Jan. 2019, doi: 10.1109/TAP.2018.2876706.

[3] D. Samantaray and S. Bhattacharyya, "A gain-enhanced slotted patch antenna using metasurface as superstrate configuration," *IEEE Trans. Antennas Propag.*, vol. 68, no. 9, pp. 6548–6556, Sep. 2020, doi: 10.1109/TAP.2020.2990280.

[4] D. Samantaray, S. Bhattacharyya, and K. V. Srinivas, "A modified fractal-shaped slotted patch antenna with defected ground using metasurface for dual band applications," *Int. J. RF Microw. Comput.-Aided Eng.*, vol. 29, no. 12, Dec. 2019, Art. no. e21932, doi: 10.1002/mmce.21932.

[5] P. Munaga, S. Bhattacharyya, S. Ghosh, and K. V. Srivastava, "An ultra-thin compact polarization-independent hexa-band metamaterial absorber," *Appl. Phys. A, Solids Surf.*, vol. 124, no. 4, p. 331, Mar. 2018, doi: 10.1007/s00339-018-1751-x.

[6] D. Chaurasiya, S. Ghosh, S. Bhattacharyya, S. Bhattacharyya, A. Bhattacharya, and K. V. Srivastava, "Compact multi-band polarisation-insensitive metamaterial absorber," *IET Microw., Antennas Propag.*, vol. 10, no. 1, pp. 94–101, Jan. 2016, doi: 10.1049/iet-map.2015.0220.

[7] Z. Zhang, X. Cao, J. Gao, and S. Li., "Broadband metamaterial reflectors for polarization manipulation based on Cross/Ring resonators," *Radioengineering*, vol. 25, no. 3, pp. 436–441, Sep. 2016, doi: 10.13164/re.2016.0436.

[8] S. Bhattacharyya, S. Ghosh, and K. V. Srivastava, "A wideband cross polarization conversion using metasurface," *Radio Sci.*, vol. 52, no. 11, pp. 1395–1404, Nov. 2017, doi: 10.1002/2017RS006396.

[9] M. I. Khan, Q. Fraz, and F. A. Tahir, "Ultra-wideband cross polarization conversion metasurface insensitive to incidence angle," *J. Appl. Phys.*, vol. 121, no. 4, Jan. 2017, Art. no. 045103, doi: 10.1063/1.4974849.

[10] H. Chen, J. Wang, H. Ma, S. Qu, Z. Xu, A. Zhang, M. Yan, and Y. Li, "Ultra-wideband polarization conversion metasurfaces based on multiple plasmon resonances," *J. Appl. Phys.*, vol. 115, no. 15, Apr. 2014, Art. no. 154504, doi: 10.1063/1.4869917.

[11] Q. Zheng, C. Guo, and J. Ding, "Wideband metasurface-based reflective polarization converter for linear-to-linear and linear-to-circular polarization conversion," *IEEE Antennas Wireless Propag. Lett.*, vol. 17, no. 8, pp. 1459–1463, Aug. 2018, doi: 10.1109/LAWP.2018.2849352.

[12] M. S. Salman, M. I. Khan, F. A. Tahir, and H. Rmili, "Multi-functional single layer metasurface based on hexagonal split ring resonator," *IEEE Access*, vol. 8, pp. 28054–28063, Feb. 2020, doi: 10.1109/ACCESS.2020.2971557.

[13] D. J. Liu, Z. Y. Xiao, and Z. H. Wang, "Multi-band asymmetric transmission and 90° polarization rotator based on bi-layered metasurface with F-shaped structure," *Plasmonics*, vol. 12, no. 2, pp. 445–452, Apr. 2017, doi: 10.1007/s11468-016-0284-4.

[14] Y. Yuan, S. Sun, Y. Chen, K. Zhang, X. Ding, B. Ratni, Q. Wu, S. N. Burokur, and C.-W. Qiu, "A fully phase-modulated metasurface as an energy-controllable circular polarization router," *Adv. Sci.*, vol. 7, no. 18, Jul. 2020, Art. no. 2001437, doi: 10.1002/advs.202001437.

[15] K. Zhang, , Y. Yuan, X. Ding, B. Ratni, S. N. Buroku, and Q. Wu, "High-efficiency metalenses with switchable functionalities in microwave region," *ACS Appl. Mater. Interfaces*, vol. 11, no. 31, pp. 28423–28430, Aug. 2019, doi: 10.1021/acsami.9b07102.

[16] S. Li, Y. B. Li, H. Li, Z. X. Wang, C. Zhang, Z. X. Guo, R. Q. Li, X. Y. Cao, Q. Cheng, and T. J. Cui, "A thin self-feeding Janus metasurface for manipulating incident waves and emitting radiation waves simultaneously," *Annalen der Physik*, vol. 532, no. 5, Apr. 2020, Art. no. 2000020, doi: 10.1002/andp.202000020.

[17] S. Li, Y. B. Li, R. Q. Li, Q. Cheng, and T. J. Cui, "Digital-coding-feeding metasurfaces for differently polarized wave emission, orbit angular momentum generation, and scattering manipulation," *Adv. Photon. Res.*, vol. 1, no. 1, Nov. 2020, Art. no. 2000012, doi: 10.1002/adpr.202000012.

[18] Y. Yuan, K. Zhang, B. Ratni, Q. Song, X. Ding, Q. Wu, S. N. Burokur, and P. Genevet, "Independent phase modulation for quadruplex polarization channels enabled by chirality-assisted geometric-phase metasurfaces," *Nature Commun.*, vol. 11, no. 1, p. 4186, Aug. 2020, doi: 10.1038/s41467-020-17773-6.

[19] J. Poojali, S. Ray, B. Pesala, K. C. Venkata, and K. Arunachalam, "Quad-band polarization-insensitive millimeter-wave frequency selective surface for remote sensing," *IEEE Antennas Wireless Propag. Lett.*, vol. 16, pp. 1796–1799, Mar. 2017, doi: 10.1109/LAWP.2017.2679204.

[20] S. S. Sampath, R. Sivasamy, and K. J. J. Kumar, "A novel miniaturized polarization independent band-stop frequency selective surface," *IEEE Trans. Electromagn. Compat.*, vol. 61, no. 5, pp. 1678–1681, Oct. 2019, doi: 10.1109/TEMC.2018.2869664.

[21] E. Arnieri, F. Greco, L. Boccia, and G. Amendola, "A SIW-based polarization rotator with an application to linear-to-circular dual-band polarizers at $K - -/Ka$-band," *IEEE Trans. Antennas Propag.*, vol. 68, no. 5, pp. 3730–3738, May 2020, doi: 10.1109/TAP.2020.2963901.

[22] A. A. Omar, Z. Shen, and S.-Y. Ho, "Multiband and wideband 90° polarization rotators," *IEEE Antennas Wireless Propag. Lett.*, vol. 17, no. 10, pp. 1822–1826, Oct. 2018, doi: 10.1109/LAWP.2018.2867489.

[23] M. Saikia, S. Ghosh, and K. V. Srivastava, "Design and analysis of ultrathin polarization rotating frequency selective surface using V-Shaped slots," *IEEE Antennas Wireless Propag. Lett.*, vol. 16, pp. 2022–2025, 2017, doi: 10.1109/LAWP.2017.2693685.

[24] X. Liu, X. Cao, J. Yu, X. Chen, Y. Yao, L. Qi, Z. Chen, and J. Zhou, "Polarization rotator of arbitrary angle based on simple slot-array," *AIP Adv.*, vol. 5, no. 12, Dec. 2015, Art. no. 127142, doi: 10.1063/1.4939582.

[25] D. M. Pozar, *Microwave Engineering*, 3rd ed. New York, NY, USA: Wiley, 2005, ch. 3.
[26] B. A. Munk, *Frequency Selective Surfaces: Theory and Design*. New York, NY, USA: Wiley, 2005.
[27] M. A. Al-Joumayly and N. Behdad, "Low-profile, highly-selective, dual-band frequency selective surfaces with closely spaced bands of operation," *IEEE Trans. Antennas Propag.*, vol. 58, no. 12, pp. 4042–4050, Dec. 2010, doi: 10.1109/TAP.2010.2078478.
[28] X. Liu, S. Yu, L. Gan, and J. Yu, "Broadband quasi-optical dielectric spectroscopy for solid and liquid samples," *J. Infr., Millim., Terahertz Waves*, vol. 41, no. 7, pp. 810–824, Jul. 2020, doi: 10.1007/s10762-020-00710-5.
[29] X. Yang, X. Liu, S. Yu, L. Gan, J. Zhou, and Y. Zeng, "Permittivity of undoped silicon in the millimeter wave range," *Electronics*, vol. 8, no. 8, p. 886, Aug. 2019, doi: 10.3390/electronics8080886.
[30] L. Nama, S. Bhattacharyya, and P. Chakrabarti, "A metasurface-based broadband quasi nondispersive cross polarization converter for far infrared region," *Int. J. RF Microw. Comput.-Aided Eng.*, vol. 29, no. 10, Oct. 2019, Art. no. e21889, doi: 10.1002/mmce.21889.
[31] S. A. Winkler, W. Hong, and M. Bozzi, "Polarization rotating frequency selective surface based on substrate integrated waveguide technology," *IEEE Trans. Antennas Propag.*, vol. 58, no. 4, pp. 1202–1213, Apr. 2010, doi: 10.1109/TAP.2010.2041170.

**XIAOMING LIU** (Member, IEEE) received the B.Sc. degree in applied physics from the Nanjing University of Posts and Telecommunications, Nanjing, China, in 2006, and the Ph.D. degree in electronic engineering from the School of Electronic Engineering and Computer Science, Queen Mary University of London, London, U.K., in 2012.

In 2012, he joined the School of Electronic Engineering, Beijing University of Posts and Telecommunications. He is currently with the School of Physics and Electronic Information, Anhui Normal University. His research interests include terahertz science and technology, quasi-optical techniques and systems, millimeter and sub-millimeter wave antenna measurement techniques and bio-electromagnetics.

**TAO QI** received the bachelor's degree from the Wanjiang College, Anhui Normal University, Anhui, China, in 2018. He is currently studying in the School of Physics and Electronic Information, Anhui Normal University. His researches focus on millimeter wave components and antenna measurement technology.

**CHEN WANG** received the master's degree in engineering from Anhui Normal University, in 2017. He works with the School of Computer and Information, Anhui Normal University, where he is currently pursuing the Ph.D. degree with the School of Physics and Electronic Information. His research interests include terahertz science and technology, millimeter and sub-millimeter wave antenna measurement techniques, and electronic circuit technology.

**XIAOFAN YANG** received the Ph.D. degree in electromagnetic and microwave technology from the School of Electronic Science and Engineering, University of Electronic Science and Technology of China, in 2012.

During the doctoral student, he joined the EHF Key Laboratory of Fundamental Science, University of Electronic Science and Technology of China. From 2011 to 2012, he has been titled as a Visiting Scientist to RAL Space, Rutherford Appleton Laboratory, Science and Technology Facilities Council, Oxford, U.K. He is currently with the State Key Laboratory of Complex Electromagnetic Environment Effects on Electronics and Information System, Luoyang Electronic Equipment Test Center of China. His research interests include terahertz science and technology, electromagnetic wave propagation, millimeter and sub-millimeter wave receiver front-end.

**LU GAN** received the Ph.D. degree in pattern recognition and intelligent system from Xidian University, Xi'an, China, in 2015. In 2015, he joined the School of Physics and Electronic Information, Anhui Normal University. His research interests include image processing, machine learning, millimeter wave and terahertz imaging technology.

**QING CAI** received the M.S. degree in testing technology and automatic equipment from the University of Shanghai for Science and Technology, Shanghai, China, in 2005.

In 2005, she joined the Shanghai Institute of Measurement and Testing Technology (SIMT). She is currently working with the Institute of Electron and Electric Measurement Technology in SIMT. Her research interests include measurement technology of electromagnetic materials and dielectric characteristics of electromagnetic materials.